Applied Physics Letters

Experimental verification of semi-metallic band structure in $PtSe_2$ via thermoelectric power measurements

Cite as: Appl. Phys. Lett. **120**, 043103 (2022); https://doi.org/10.1063/5.0076972
Submitted: 29 October 2021 • Accepted: 07 January 2022 • Published Online: 24 January 2022

Jeongmin Kim, Seonhye Youn, Joonho Bang, et al.

Applied Physics Letters ARTICLE scitation.org/journal/apl

Experimental verification of semi-metallic band structure in $PtSe_2$ via thermoelectric power measurements

Cite as: Appl. Phys. Lett. **120**, 043103 (2022); doi: 10.1063/5.0076972
Submitted: 29 October 2021 · Accepted: 7 January 2022 ·
Published Online: 24 January 2022

Jeongmin Kim,[1] Seonhye Youn,[2] Joonho Bang,[3] Hongjae Moon,[2] Woosun Jang,[4] Jong Wook Roh,[5] Dong Hwan Kim,[1] Joonyeon Chang,[2,6] and Wooyoung Lee[2,7,a)]

AFFILIATIONS

[1]Division of Nanotechnology, DGIST, 333 Techno Jungang-daero, Hyeonpung-eup, Dalseong-gun, Daegu 42988, South Korea
[2]Department of Materials Science and Engineering, Yonsei University, 50 Yonsei-ro, Seodaemoon-gu, Seoul 03722, South Korea
[3]Department of Energy Science, Sungkyunkwan University, Suwon 16419, South Korea
[4]Center for Artificial Synesthesia Materials Discovery, Yonsei University, Seoul 03722, South Korea
[5]School of Nano Materials Engineering, Kyungpook National University, Gyeongsangbuk-do 37224, South Korea
[6]Natural Products Institute, Korea Institute of Science and Technology (KIST), 679 Saimdang-ro, Gangneung, Gangwon-do 25451, South Korea
[7]Center for Spintronics, Post-silicon Semiconductor Insitute, Korea Institute of Science and Technology, Seoul 02792, South Korea

Note: This paper is part of the APL Special Collection on Thermoelectric Materials Science and Technology Towards Applications.
[a)]**Author to whom correspondence should be addressed:** wooyoung@yonsei.ac.kr

ABSTRACT

We present an investigation of the band structure in the semi-metallic two-dimensional (2D) $PtSe_2$ based on thermoelectric transport phenomena. The gate-tuned electrical conductivity and thermoelectric power were measured by varying the temperature using mechanically exfoliated $PtSe_2$ nanosheets, including naturally doped non-neutral samples. Through the synergy of the gate-tuning effect and shifted zero-gate energy level, the semi-metallic band structure of 2D $PtSe_2$ was confirmed by the transport properties in the band over a wide energy range. The temperature dependence of the transport properties was also investigated to determine the band structure and intrinsic properties.

Two-dimensional (2D) transition metal dichalcogenides (TMDCs) have attracted great attention since the discovery of graphene through mechanical exfoliation because of their unique properties and electronic structures.[1–4] In particular, significant efforts have been made to enhance the thermoelectric performance using the potential of simple and clear band engineering in TMDCs based on thickness control.[5–11] Recently, a large thermoelectric power factor ($S^2\sigma$) comparable to that of the commercial bulk Bi_2Te_3 was reported for 2D TMDCs with a semiconducting band structure (WSe_2, MoS_2, and black phosphorus), where S and σ are the thermoelectric power (TEP) and electrical conductivity, respectively.[5–7] The enhancement of the power factor was theoretically predicted for various semiconducting TMDCs (MoS_2, $MoSe_2$, WS_2, SnS_2, and TiS_2).[8–11] In contrast, the thermoelectric properties have been used to understand the electronic structures of low-dimensional materials, because TEP depends very sensitively on the type of carriers and the band structure of the materials.[12] Using TEP measurements, diameter-dependent band engineering was demonstrated for 1D materials,[12,13] and the surface states and doping effects were elucidated for a 2D topological insulator and a 2D metal oxide, respectively.[14,15] Particularly, the zero-mass, zero-gap, and ambipolar nature of graphene could be directly observed through the gate-tuned TEP measurement.[16] Moreover, the change in the bandgap caused by the thickness reduction in semiconducting 2D TMDCs was experimentally evaluated using gate-tuned TEP measurements.[5–7] Recently, dramatic band structure engineering was demonstrated using a semimetal TMDC ($PtSe_2$) based on thickness modulation. The semimetal-to-semiconductor transition, which was theoretically predicted for monolayer $PtSe_2$, was clearly observed by thermoelectric transport measurements.[17–19] Moreover, TEP and a power factor that significantly exceed the bulk values were obtained

for bilayer $PtSe_2$.[20] After the transition to the semiconductor 2D $PtSe_2$, the monopolar transport phenomena of both the conduction and valence bands could be independently observed by gate-tuning without minor carrier compensation due to bandgap formation.[19,20] In contrast, for semi-metallic 2D $PtSe_2$, single-band transport was hardly observed because of the presence of intrinsic bipolar carriers owing to band overlap.[18,20] Therefore, it was challenging to examine the band structure over a wide energy range across the neutral point using single gate-tuned TEP measurements, which were successfully performed on zero-gap graphene.[16] In this study, we investigated the band structure of semi-metallic 2D $PtSe_2$ through gate-tuned electrical conductivity and TEP measurements. To observe the transport phenomena up to the energy region at which there is no minor carrier compensation, five different $PtSe_2$ nanosheets, including naturally doped non-neutral samples, were employed in the gate-tuned measurements. Through the synergy of the gate-tuning effect and shifted zero-gate energy level of the non-neutral samples, we were able to experimentally verify the entire semi-metallic band of 2D $PtSe_2$, including the single-band state of both the conduction and valence bands. We also discuss the temperature dependence of the gate-tuned transport phenomena in the investigation of the band structure and the intrinsic properties.

$PtSe_2$ crystals have a layered structure in which the layers are held together by weak interlayer van der Waals forces, but the intralayer atoms are strongly connected to each other by covalent bonds [Fig. 1(a)].[21,22] Therefore, 2D $PtSe_2$ nanosheets can be obtained by mechanical exfoliation using adhesive tapes from $PtSe_2$ crystals (HQ Graphene). Figure 1(b) shows a scanning electron microscopy (SEM, 7800F, JEOL) image of the exfoliated $PtSe_2$ nanosheets dispersed on a doped Si substrate covered with 300 nm of SiO_2. The layered structure of the $PtSe_2$ nanosheet was directly observed from the crystallographic cracking of the nanosheets during the mechanical exfoliation process. Each $PtSe_2$ layer was composed of three sublayers of Se/Pt/Se, and a Pt atom was surrounded by six Se atoms.[18] The 1T phase atomic arrangement of $PtSe_2$ nanosheets was confirmed using an exfoliated nanosheet and a vertically sliced crystal with scanning transmission electron microscopy (STEM, JEM-ARM 200F, JEOL) and a focused ion beam (FIB, crossbeam 540, ZEISS) [Figs. 1(c) and 1(d)]. The interplanar spacings of the (100) and (001) planes were consistent with the lattice constants reported in a previous study ($a = 3.727$ Å and $c = 5.07$ Å).[23] To investigate the transport properties, including the electrical conductivity and TEP, a micro-heater, thermometers, and 4-point leads were patterned onto the dispersed nanosheet using the common electron beam lithography technique [Fig. 1(e)]. The patterned windows on the nanosheet were subjected to Ar plasma treatment (20 s) before Cr (5 nm)/Au (100 nm) metallization using a custom-made dry etching and sputtering system. The device fabrication process has been described in detail elsewhere.[12,20]

First, we performed first-principle density functional theory (DFT) calculations to obtain the band structure of the $PtSe_2$ crystal using the Vienna *ab initio* simulation program code.[24] Figure 2(a) shows the clear semi-metallic band structure of bulk $PtSe_2$, for which the indirect band overlap energy was found to be 0.87 eV. This value was consistent with previous results obtained for the same system.[17,18] The band overlap is caused by the strong hybridization of the interlayer p_z orbital of the Se atom in $PtSe_2$.[18] Therefore, the band overlap energy decreases with a decrease in the number of $PtSe_2$ layers and is converted into a bandgap for less than three layers.[20] We estimated

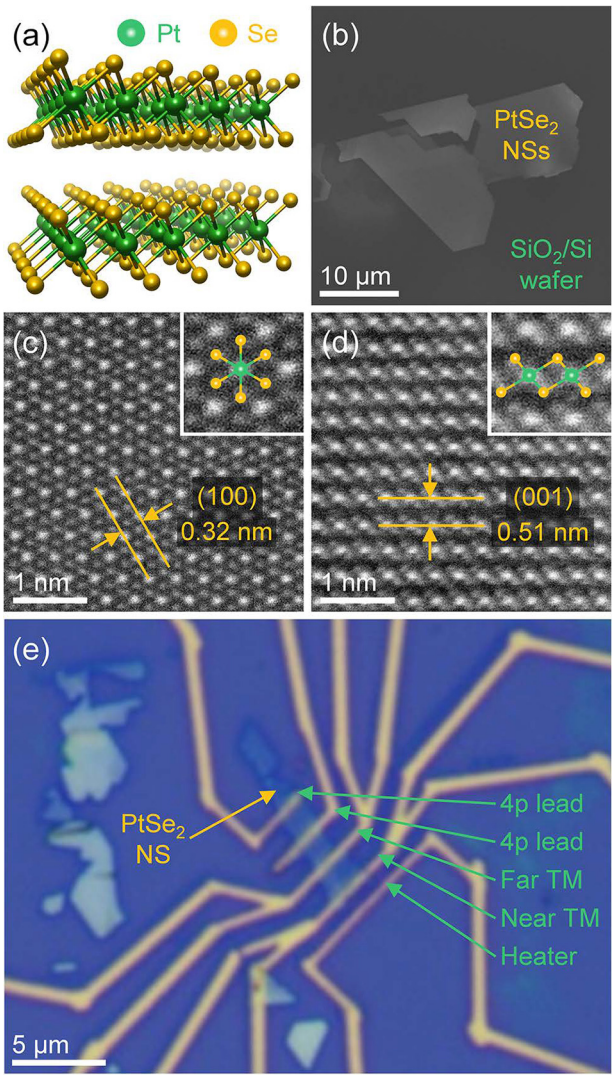

FIG. 1. (a) Schematics of the $PtSe_2$ layered crystal structure. Green and yellow spheres represent Pt and Se atoms, respectively. (b) Scanning electron microscopy (SEM) image of $PtSe_2$ nanosheets dispersed on a SiO_2/Si substrate. (c) Top and (d) side view crystal structure images of $PtSe_2$ nanosheets obtained by high-resolution scanning transmission electron microscopy (HR-STEM). Insets show the atomic arrangement. (e) Optical microscopy image of a $PtSe_2$ nanosheet device for the measurement of transport properties.

the transport properties of the $PtSe_2$ crystal by solving the Boltzmann transport equation with the Boltz TraP2 code based on DFT calculations. Figures 2(b) and 2(c) show the electrical conductivity and TEP behavior near the neutral point, respectively, which represent typical ambipolar transports in semi-metallic bands. The electrical conductivity increased monotonically on both sides of the minimum value of conductivity with an increasing density of holes and electrons, respectively. In the case of TEP, the absolute value depended on the carrier density near the neutral point according to the minor carrier compensation, whereas it was converted to a single-band feature at both ends, for which the absolute TEP decreased with the decreasing carrier

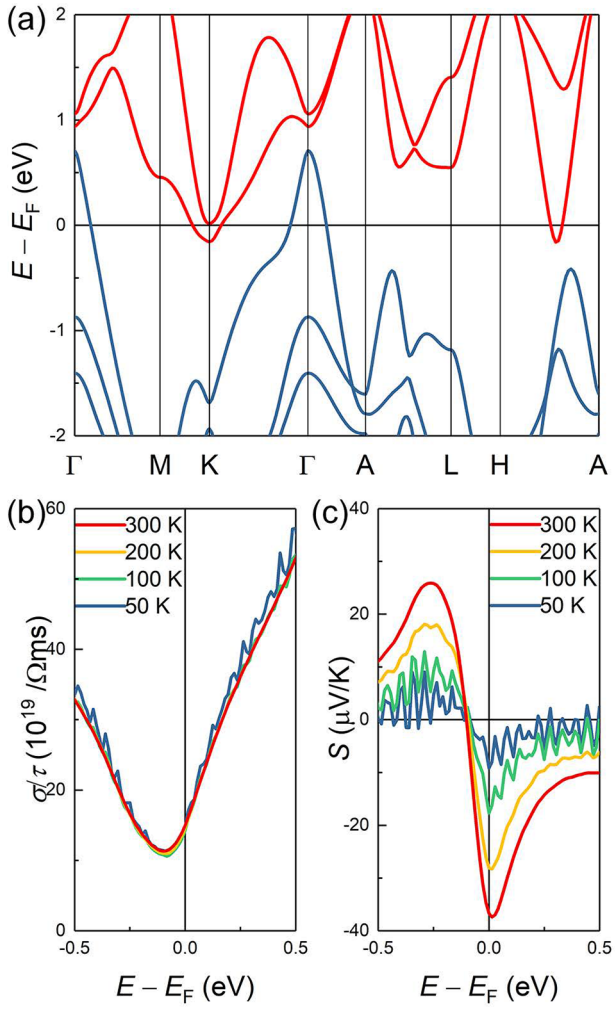

FIG. 2. (a) Electronic band structure of the $PtSe_2$ crystal obtained from first-principle density functional theory (DFT) calculations. (b) Electrical conductivity with respect to scattering time and (c) thermoelectric power (TEP) of $PtSe_2$ crystal calculated by solving the Boltzmann transport equation based on the DFT calculation.

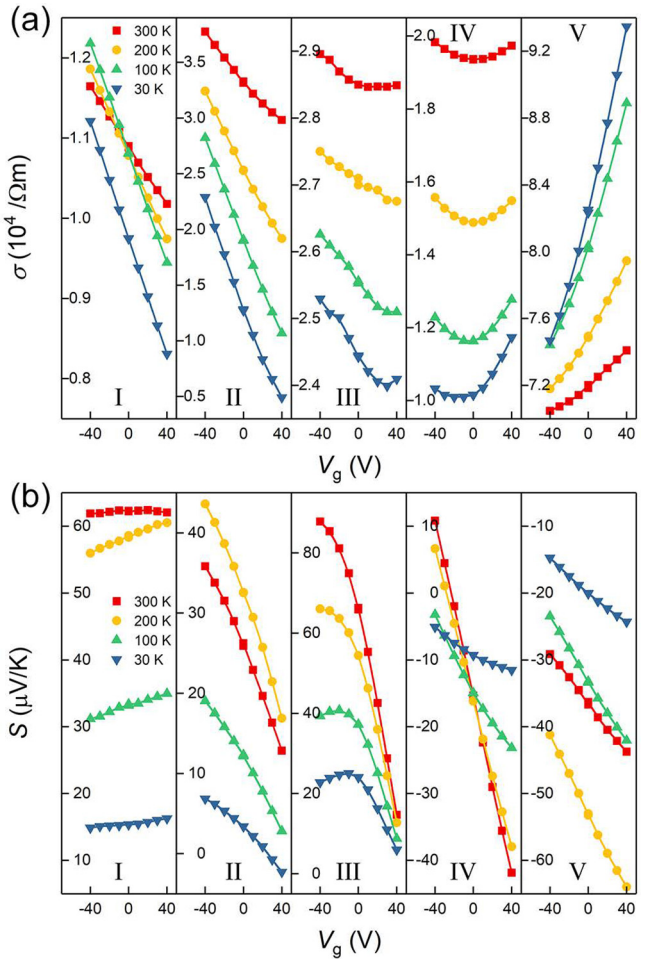

FIG. 3. (a) Gate-tuned electrical conductivity and (b) gate-tuned TEP of five different $PtSe_2$ nanosheets at 300 K (red squares), 200 K (yellow circles), 100 K (green upward-pointing triangles), and 30 K (blue downward-pointing triangles). Data were presented in the following order: from the Fermi energy shift toward the valence band, then toward the conduction band (I–V).

density. A theoretical estimation of the carrier density-dependent transport clearly reflected the semi-metallic band structure obtained for the $PtSe_2$ crystal by the DFT calculations. However, the high band overlap energy of the $PtSe_2$ crystal cannot be used for the verification of the band structure based on gate-tuned transport measurements. In studies on $PtSe_2$ nanosheets thicker than 20 layers (>10 nm), the gate-tuned transport exhibited metallic behavior for a highly degenerated band overlap.[18,20] Therefore, to expose the semi-metallic feature of the transport phenomena by reducing the band overlap energy, $PtSe_2$ nanosheets with a thickness between 3 and 10 nm were employed in the gate-tuned transport measurements.

Figures 3(a) and 3(b) show the electrical conductivity and TEP obtained from five different $PtSe_2$ nanosheets as a function of gate voltage from −40 to 40 V, respectively. Although nanosheets with less than 20 layers [thicknesses of 8.6, 3.5, 7.0, 4.6, and 5.8 nm from (I) to (V) in Fig. 3] were used to obtain gate-dependent transport, the carrier density modulation caused by the gate voltage range was insufficient for an extensive investigation of the semi-metallic band structure. Separately, we recognized that non-neutral $PtSe_2$ nanosheets were found in the gated measurements after device fabrication with a probability of approximately 20%. The shifted Fermi energy at the zero-gate voltage appeared in both the valence and conduction bands. These non-neutral $PtSe_2$ were likely due to defects in the nanosheet surface, such as the evaporation of Se atoms and oxidation, which were caused by unintentional exposure to ambient conditions for a long time during device fabrication.[25,26] Using non-neutral $PtSe_2$ nanosheets, transport measurements could be conducted over a wide energy range of the semi-metallic band structure.

First, using a strongly *p*-type shifted nanosheet, the single-band characteristics of the valence band were confirmed without minor carrier compensation [(I) in Fig. 3]. In this nanosheet, the electrical conductivity increased almost linearly with an increase in hole density according to the negative electric field effect. Moreover, the TEP

monotonically decreased with a negative gate voltage below 300 K. This behavior was weakly observed even at room temperature. The gate-tuned TEP being inversely proportional to the carrier density could be explained by the relation TEP $\sim (1/n)^{2/3}$, simplified from the Mott relation for a highly degenerate semiconductor, where n is the carrier density.[27] This clearly indicates the absence of minor carriers.[16,28] The second nanosheet also showed p-type characteristics within the gate sweep range in which the electrical conductivity monotonically increased with an increase in hole density [(II) in Fig. 3]. However, the TEP increased in proportion to the carrier density, revealing minor carrier compensation due to the participation of the secondary band. In the two-band system, the TEP of the major carriers is compensated by that of the minor carriers weighted by their partial conductivity according to the relation $S = (\sigma_h S_h + \sigma_e S_e)/(\sigma_h + \sigma_e)$, where the subscripts h and e denote holes and electrons, respectively.[28] Therefore, TEP, which is proportional to the hole density, indicates that transport occurs within the overlapped bands, despite the p-type behavior. The third nanosheet was also found to be p-type, but a minimum value point was observed in the electrical conductivity at a positive gate voltage [(III) in Fig. 3]. Although the minimum point was not exactly equal to the neutral point owing to carrier mobility (μ, $\sigma \sim n_h\mu_h + n_e\mu_e$), this observation suggests that the Fermi energy shift toward the valence band is much weaker than in the other nanosheets. Unusually, in this nanosheet, a non-monotonic variation of TEP caused by the disappearance of minor carriers was observed at low temperatures. This fact suggests that the carrier density modulation due to the field effect differs from sample to sample.

Next, we present the gate-tuned transport properties of a neutral $PtSe_2$ nanosheet [(IV) in Fig. 3]. The electrical conductivity exhibited a u-shape owing to a change in the type of major carriers within the gate sweep range, and the minimum conductivity was located near the zero-gate voltage, as shown in the theoretical calculations. The transition of the major carrier type was observed more directly in the continuous variation of TEP from positive to negative values according to the gate sweep. In this nanosheet, a negative TEP was measured at the zero-gate voltage, and the fact that the neutral $PtSe_2$ exhibits n-type characteristics regardless of thickness had been confirmed in previous studies.[18–20] Finally, a strongly n-type shifted $PtSe_2$ nanosheet was selected for the gate-tuned transport measurements [(V) in Fig. 3]. The electrical conductivity increased monotonically with an increase in the gate voltage without the minimum point. Furthermore, the increase in electron density was reflected in the temperature dependence of the electrical conductivity, which is discussed in detail in the next section. Although the single-band feature observed in the strongly p-type shifted nanosheet [(I) in Fig. 3] was not obtained, the negative values of TEP were confirmed throughout the gate sweep range.

Figure 4 shows the gate-tuned transport properties of the five different $PtSe_2$ nanosheets as a function of temperature. The electrical conductivity was normalized with respect to the value obtained at 300 K for direct comparison of the temperature dependence at different gate tunings [Fig. 4(a)]. The temperature dependence of electrical conductivity is determined by the competition between the carrier density and mobility, which decreases and increases with a reduction in temperature, respectively.[12,29] Generally, the transport in semiconductors is dominated by thermally excited carriers and, thus, exhibits carrier density dependence. In contrast, in typical metals and degenerate semiconductors, the mobility dependence caused by thermal

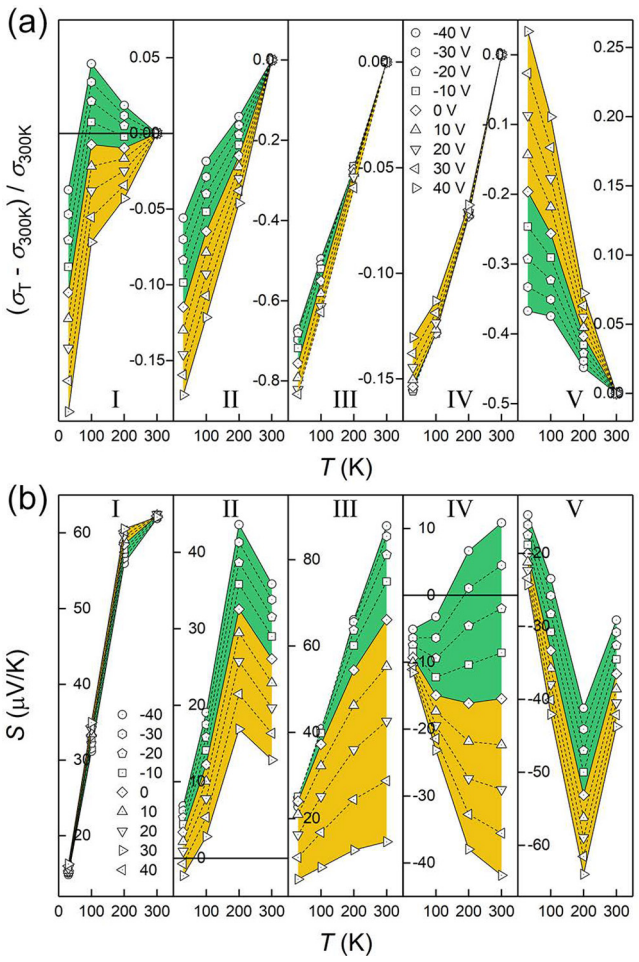

FIG. 4. (a) Temperature dependence of gate-tuned electrical conductivity and (b) gate-tuned TEP obtained from the five different $PtSe_2$ nanosheets. The electrical conductivity was normalized using the value obtained at 300 K. Data were presented in the following order: from the Fermi energy shift toward the valence band, then toward the conduction band (I–V). The circles, hexagons, pentagons, squares, rhombuses, upward-pointing, downward-pointing, left-pointing, and right-pointing triangles denote the gate voltages of −40, −30, −20, −10, 0, 10, 20, 30, and 40 V, respectively. The green and yellow regions represent the negative and positive gate sweeps, respectively.

scattering is dominant because of the sufficient intrinsic carrier density. In the case of semi-metal $PtSe_2$, both temperature behaviors were observed according to the thickness of the nanosheet owing to a change in band overlap energy.[18–20] The transition of the temperature dependence was evident around a layer number of 20; therefore, for nanosheets thinner than 10 nm used in this study, a monotonic decrease in the electrical conductivity was observed near the neutral point as the temperature decreased [(II), (III), and (IV) in Fig. 4(a)]. In these nanosheets, the slope of the temperature dependence was slightly reduced according to the additional major carriers induced by gate tuning (green for holes and yellow for electrons). However, for the strongly p-type shifted nanosheet, metallic behavior was observed at the negative gate voltages (green) at temperatures of 100–300 K [(I) in Fig. 4(a)]. Furthermore, the strongly n-type shifted nanosheet

exhibited metallic features at all temperatures, and the slope was steeper owing to positive gate voltages (yellow) [(V) in Fig. 4(a)]. These results suggest that a sufficiently high carrier density suppressed the temperature dependence.

TEP physically represents the entropy transported by a unit charge.[16] As a result, the magnitude of TEP in $PtSe_2$ nanosheets tends to decrease toward the cryogenic temperature regardless of the carrier type [Fig. 4(b)]. However, the temperature dependence of TEP shows further complex aspects in semi-metals, because the signs of the partial TEP of holes and electrons are opposite and their contribution is weighted by the partial conductivity.[28,30] Owing to the asymmetry of the temperature-dependent intrinsic properties, non-monotonic variations [(II) and (V) in Fig. 4(b)] and sign changes [(II) and (IV) in Fig. 4(b)] could be observed in the temperature dependence of TEP in two-band systems.[15,31] With the minor carrier compensation caused by the secondary band, the TEP values shifted upward and downward according to the negative (green) and positive (yellow) gate voltages [(II)–(IV) in Fig. 4(b)]. In contrast, (I) in Fig. 4 shows that TEP decreases with an increase in the number of major carriers (holes), which proves the single-band state due to the strong *p*-type shift.

In summary, the band structure of semi-metallic 2D $PtSe_2$ was investigated using changes in electrical conductivity and TEP according to variations in the gate voltage and temperature. The transport phenomena occurring in the wide energy range of the band structure could be measured using five $PtSe_2$ nanosheets, including naturally doped non-neutral samples, despite the limited charge transfer of the field effect based on the back gate. In the neutral $PtSe_2$ nanosheet, ambipolar transport due to the harmony between holes and electrons in the two-band system was confirmed, which is consistent with previous studies. Moreover, gate-tuned transports in the *p*-type and *n*-type shifted nanosheets clearly exhibited major carrier dependence within the minor carrier compensation effect. Furthermore, with a strongly *p*-type shifted nanosheet, single-band transport phenomena were first obtained from semi-metallic 2D $PtSe_2$. Our observations experimentally verified the semi-metallic band structure of $PtSe_2$ and demonstrated that thermoelectric measurements can be used to understand veiled 2D materials.

This work was supported by the Yonsei-KIST Institutional Program (Project No. 2Z06430-20-P069), the Technology Innovation Program ("20013621," Center for Super Critical Material Industrial Technology) funded by the Ministry of Trade, Industry & Energy (MOTIE, Korea), and the Basic Science Research Program through the National Research Foundation of Korea (NRF) (No. NRF-2019R1A6A1A11055660). J.K. acknowledges support from the National Research Foundation of Korea (NRF) (Nos. NRF-2019R1I1A1A01063687 and NRF-2021R1A5A8033165) and by the DGIST R&D Program (No. 21-ET-07).

AUTHOR DECLARATIONS

Conflict of Interest

The authors have no conflicts to disclose.

Author Contributions

J.K. and S.Y. contributed equally to this work.

DATA AVAILABILITY

The data that support the findings of this study are available within the article.

REFERENCES

[1]K. S. Novoselov, A. K. Geim, S. V. Morozov, D. Jiang, M. I. Katsnelson, I. V. Grigorieva, S. V. Dubonos, and A. A. Firsov, Nature **438**(7065), 197–200 (2005).
[2]A. K. Geim and K. S. Novoselov, Nat. Mater. **6**(3), 183–191 (2007).
[3]Q. H. Wang, K. Kalantar-Zadeh, A. Kis, J. N. Coleman, and M. S. Strano, Nat. Nano **7**(11), 699–712 (2012).
[4]M. Chhowalla, H. S. Shin, G. Eda, L.-J. Li, K. P. Loh, and H. Zhang, Nat. Chem. **5**(4), 263–275 (2013).
[5]M. Yoshida, T. Iizuka, Y. Saito, M. Onga, R. Suzuki, Y. Zhang, Y. Iwasa, and S. Shimizu, Nano Lett. **16**(3), 2061–2065 (2016).
[6]K. Hippalgaonkar, Y. Wang, Y. Ye, D. Y. Qiu, H. Zhu, Y. Wang, J. Moore, S. G. Louie, and X. Zhang, Phys. Rev. B **95**(11), 115407 (2017).
[7]M. Park, S. J. Hong, K. H. Kim, H. Kang, M. Lee, D. H. Jeong, Y. W. Park, and B. H. Kim, Appl. Phys. Lett. **111**(17), 173103 (2017).
[8]D. Wickramaratne, F. Zahid, and R. K. Lake, J. Chem. Phys. **140**(12), 124710 (2014).
[9]W. Huang, X. Luo, C. K. Gan, S. Y. Quek, and G. Liang, Phys. Chem. Chem. Phys. **16**(22), 10866–10874 (2014).
[10]J. Li, J. Shen, Z. Ma, and K. Wu, Sci. Rep. **7**(1), 8914 (2017).
[11]R.-Z. Zhang, C.-L. Wan, Y.-F. Wang, and K. Koumoto, Phys. Chem. Chem. Phys. **14**(45), 15641–15644 (2012).
[12]J. Kim, S. Lee, Y. M. Brovman, P. Kim, and W. Lee, Nanoscale **7**, 5053–5059 (2015).
[13]J. Kim, M.-W. Oh, G. Kim, J.-H. Bahk, J. Y. Song, S. G. Jeon, D. W. Chun, J.-H. Bae, W. Shim, and W. Lee, Acta Mater. **144**, 145–153 (2018).
[14]D. Kim, P. Syers, N. P. Butch, J. Paglione, and M. S. Fuhrer, Nano Lett. **14**(4), 1701–1706 (2014).
[15]J. Kim, S. Yoo, H. Moon, S. Y. Kim, D. S. Ko, J. W. Roh, and W. Lee, Nanotechnology **29**(1), 015404 (2018).
[16]Y. M. Zuev, W. Chang, and P. Kim, Phys. Rev. Lett. **102**(9), 096807 (2009).
[17]S.-D. Guo, J. Mater. Chem. C **4**(39), 9366–9374 (2016).
[18]Y. Zhao, J. Qiao, Z. Yu, P. Yu, K. Xu, S. P. Lau, W. Zhou, Z. Liu, X. Wang, W. Ji, and Y. Chai, Adv. Mater. **29**(5), 1604230 (2017).
[19]A. Ciarrocchi, A. Avsar, D. Ovchinnikov, and A. Kis, Nat. Commun. **9**(1), 919 (2018).
[20]H. Moon, J. Bang, S. Hong, G. Kim, J. W. Roh, J. Kim, and W. Lee, ACS Nano **13**(11), 13317–13324 (2019).
[21]L.-H. Zeng, S.-H. Lin, Z.-J. Li, Z.-X. Zhang, T.-F. Zhang, C. Xie, C.-H. Mak, Y. Chai, S. P. Lau, L.-B. Luo, and Y. H. Tsang, Adv. Funct. Mater. **28**(16), 1705970 (2018).
[22]S. Yin, W. Zhang, C. Tan, L. Chen, J. Chen, G. Li, H. Zhang, Y. Zhang, W. Wang, and L. Li, J. Phys. Chem. C **125**(29), 16129–16135 (2021).
[23]K. Zhang, M. Yan, H. Zhang, H. Huang, M. Arita, Z. Sun, W. Duan, Y. Wu, and S. Zhou, Phys. Rev. B **96**(12), 125102 (2017).
[24]G. Kresse and J. Furthmüller, Phys. Rev. B **54**(16), 11169–11186 (1996).
[25]D. Cao, H. B. Shu, T. Q. Wu, Z. T. Jiang, Z. W. Jiao, M. Q. Cai, and W. Y. Hu, Appl. Surf. Sci. **361**, 199–205 (2016).
[26]D. Kong, J. J. Cha, K. Lai, H. Peng, J. G. Analytis, S. Meister, Y. Chen, H.-J. Zhang, I. R. Fisher, Z.-X. Shen, and Y. Cui, ACS Nano **5**(6), 4698–4703 (2011).
[27]J. P. Heremans, V. Jovovic, E. S. Toberer, A. Saramat, K. Kurosaki, A. Charoenphakdee, S. Yamanaka, and G. J. Snyder, Science **321**(5888), 554–557 (2008).
[28]J. Kim, W. Shim, and W. Lee, J. Mater. Chem. C **3**(46), 11999–12013 (2015).
[29]J. Heremans, C. M. Thrush, Y. M. Lin, S. Cronin, Z. Zhang, M. S. Dresselhaus, and J. F. Mansfield, Phys. Rev. B **61**(4), 2921–2930 (2000).
[30]L. D. Hicks and M. S. Dresselhaus, Phys. Rev. B **47**(19), 12727–12731 (1993).
[31]J. Kim, J. W. Roh, H. Moon, and W. Lee, J. Appl. Phys. **122**(3), 034303 (2017).